Homotrimer Formation and Dissociation of pharaonis Halorhodopsin in Detergent System

ARTICLE *in* BIOPHYSICAL JOURNAL · JUNE 2012

Impact Factor: 3.97 · DOI: 10.1016/j.bpj.2012.05.008 · Source: PubMed

9 AUTHORS, INCLUDING:

Masakatsu Kamiya
Hokkaido University
41 PUBLICATIONS **438** CITATIONS
SEE PROFILE

Keiichi Kawano
Hokkaido University
86 PUBLICATIONS **1,069** CITATIONS
SEE PROFILE

Homotrimer Formation and Dissociation of *pharaonis* Halorhodopsin in Detergent System

Takashi Tsukamoto,[†△] Takanori Sasaki,[‡△] Kazuhiro J. Fujimoto,[§] Takashi Kikukawa,[†] Masakatsu Kamiya,[†] Tomoyasu Aizawa,[†] Keiichi Kawano,[†] Naoki Kamo,[¶] and Makoto Demura[†*]

[†]Faculty of Advanced Life Science, Hokkaido University, Sapporo, Japan; [‡]School of Science and Technology, Meiji University, Tama-ku, Kawasaki-shi, Kanagawa, Japan; [§]Department of Computational Science, Graduate School of System Informatics, Kobe University, Rokkodai, Kobe, Japan; and [¶]College of Pharmaceutical Sciences, Matsuyama University, Bunkyo-cho, Matsuyama, Japan

ABSTRACT Halorhodopsin from NpHR is a light-driven Cl^- pump that forms a trimeric NpHR-bacterioruberin complex in the native membrane. In the case of NpHR expressed in *Escherichia coli* cell, NpHR forms a robust homotrimer in a detergent DDM solution. To identify the important residue for the homotrimer formation, we carried out mutation experiments on the aromatic amino acids expected to be located at the molecular interface. The results revealed that Phe^{150} was essential to form and stabilize the NpHR trimer in the DDM solution. Further analyses for examining the structural significance of Phe^{150} showed the dissociation of the trimer in F150A (dimer) and F150W (monomer) mutants. Only the F150Y mutant exhibited dissociation into monomers in an ionic strength-dependent manner. These results indicated that spatial positions and interactions between F150-aromatic side chains were crucial to homotrimer stabilization. This finding was supported by QM calculations. In a functional respect, differences in the reaction property in the ground and photoexcited states were revealed. The analysis of photointermediates revealed a decrease in the accumulation of O, which is important for Cl^- release, and the acceleration of the decay rate in L1 and L2, which are involved in Cl^- transfer inside the molecule, in the trimer-dissociated mutants. Interestingly, the affinity of them to Cl^- in the photoexcited state increased rather than the trimer, whereas that in the ground state was almost the same without relation to the oligomeric state. It was also observed that the efficient recovery of the photocycle to the ground state was inhibited in the mutants. In addition, a branched pathway that was not included in Cl^- transportation was predicted. These results suggest that the trimer assembly may contribute to the regulation of the dynamics in the excited state of NpHR.

INTRODUCTION

Halophilic archaea have four kinds of rhodopsin-like molecules, called archaeal rhodopsins (1): bacteriorhodopsin (BR), halorhodopsin (HR), sensory rhodopsin I (SRI), and sensory rhodopsin II (SRII, also called phoborhodopsin, pR). Their tertiary structures are very similar in that they have seven transmembrane α-helices and a retinal chromophore binding to lysine, which is conserved on the seventh helix, via the protonated Schiff base. The three-dimensional structures of BR, HR, and SRII have already been revealed (2–5). These rhodopsins are classified into two functional types: photo-induced ion pumps as BR and HR, and phototaxis receptors as SRI and SRII. Archaeal rhodopsins also form intrinsic oligomers according to their functional type. Phototaxis receptors SRI and SRII form a heterotetramer, which is composed of the two units of receptor-transducer heterodimeric complex. This oligomerization is a significant process by which information is relayed from outside to inside the cell (5). On the other hand, the ion pumps BR and HR exist as a homotrimer in the archaeal cell membrane (2–4,6–9). This is one of their unique structural properties, but few reports have discussed in detail the mechanisms of trimer formation and stabilization (6–9). Moreover, the biological significance of trimeric assembly is not yet understood.

HR acts as an inward-directed chloride pump (10,11). Recently, the electrical function of NpHR has been applied to optogenetics, the technique of which has the potential to enhance the basic knowledge in neuroscience research and to inform the mechanisms and treatment of brain injury and disease (12,13). The first structural information about HR was provided by cryo-electron microscopy of tetragonal two-dimensional crystals of HsHR (14). Although this crystal was a physiologically irrelevant artifact, the structural data of up to 5 Å resolutions revealed the overall architecture of HR. A more detailed structural model of trimeric HsHR was built by Kolbe et al. (3) in 2000 by means of x-ray crystallography (Fig. 1 *A*). More recently, the trimeric NpHR-bacterioruberin complex has been isolated from the *Natronomonas pharaonis* strain KM-1 cells (15) and its crystal structure has been also revealed (Fig. 1 *B*) (4). The carotenoid bacterioruberin binds to crevices between adjacent NpHR subunits in the trimeric assembly and the central part of the trimer is filled with three lipid molecules. Although the crystal structures of HsHR and NpHR are very similar to each other (root mean-square deviation of

Submitted May 27, 2011, and accepted for publication May 8, 2012.

[△]Takashi Tsukamoto and Takanori Sasaki contributed equally to this work.

*Correspondence: demura@sci.hokudai.ac.jp

Abbreviations used: NpHR, halorhodopsin from *Natronomonas pharaonis*; HsHR, halorhodopsin from *Halobacterium salinarum*; QM/MM, quantum mechanics/molecular mechanics; *N*, *N*-intermediate; O, O-intermediate; NpHR′, NpHR′-intermediate; DDM, *n*-dodecyl-β-D-maltoside; GA, glutaraldehyde; CD, circular dichroism; SEC, size-exclusion chromatography.

Editor: Leonid S. Brown.

0006-3495/12/06/2906/10 $2.00

doi: 10.1016/j.bpj.2012.05.008

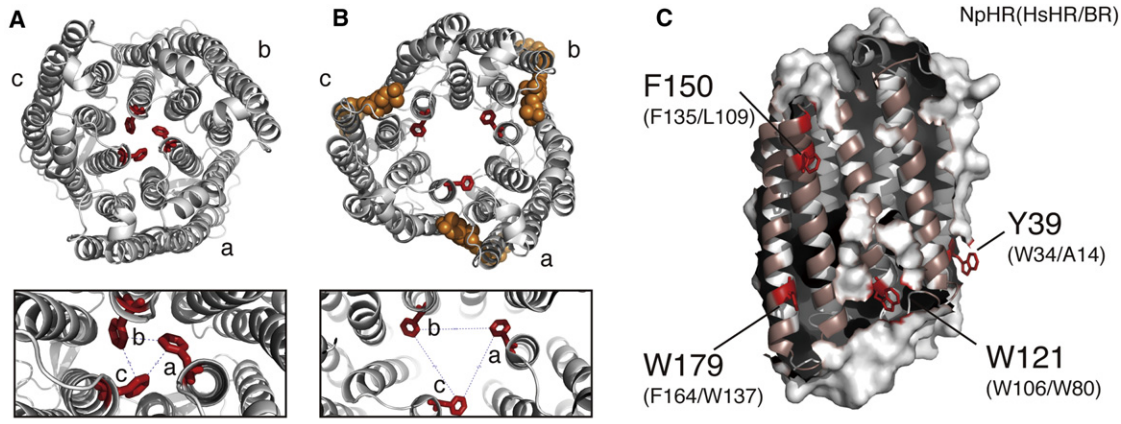

D

	39	121	150	179
NpHR	-SSLYINI-	--TMWGRY-	-TKLFTAI-	-RWFWYAI-
HsHR	-SSLWVNI-	-RSQWGRY-	-ASLFTAI-	-RWVFYGI-
Halobac sp. HR	-SSLWVNV-	-RSQWGRY-	-GSLFTVI-	-RWAFYAI-
HmHR	-SSIWVNI-	-LSPWGRY-	-ASLFTAI-	-RWVFYGI-
HvCHR	-SSLWVNI-	-LSPWGRY-	-ASLFTAI-	-RWVFYGI-
HsoHR	-SSLWINI-	-LTPWGRY-	-TKLFTAV-	-RWVWYVI-
Haloter sp. HR	-SSLWVNI-	-LSQWGRY-	-ADLFVVI-	-RWAFYLV-
HwHR	-SSLWVNI-	-MSQWGRY-	-GSLFTVI-	-RWAFYII-
SrHR	-SSIYVNI-	-LSLWGRY-	-DKIFSAI-	-RWLWYAL-
HsBR	-IWLALGT-	-PIYWARY-	-GTILALV-	-RFVWWAI-
HsSRI	-AYLGGAV-	---------	-RSIIGVM-	-KWALFGV-
NpSRII	-TLFWLGA-	-TVFVPRY-	-REFGIVI-	-RYALFGM-

*Residual numbers correspond to those of NpHR.
Np; *Natronomonas pharaonis* Hs; *Halobacterium salinarum*
Halobac sp.; *Halobacterium* species Hm; *Haloarcula marismortui*
HvCHR; *Haloarcula vallismortis* cruxhalorhodopsin-3 Hso; *Halorubrum sodomense*
Haloter sp.; *Haloterrigena* species Hw; *Haloquadratum walsbyi* Sr; *Salinibacter ruber*

FIGURE 1 (*A*) Trimeric assembly of HsHR (PDB code; 1E12) and (*B*) NpHR (PDB code; 3A7K) viewed from the cytoplasmic side. The extended figures around the center of the trimer are shown below. Homologous three aromatic side chains of HsHR-F135 and NpHR-F150 are shown in red. The crystal structure of NpHR contains the secondary pigment bacterioruberin shown as an orange sphere. (*C*) Mapping the aromatic amino acids located at the protein interface on the x-ray crystal structure of HsHR. The molecular surface corresponding to the contact region was removed. The helices in this region are shown in brown. Four aromatic amino acids, Y39, W121, F150, and W179 of NpHR, were mutated into alanine. (*D*) Sequence alignment of HRs and other archaeal rhodopsins, BR, SRI, and SRII. Amino acid sequences were derived from DDBJ. The conserved aromatic residues are highlighted in gray.

0.69 Å for all Cα atoms), HsHR monomers in the homotrimer are tilted ~11° relative to the monomers in the NpHR-bacterioruberin complex (4). In other words, there are two types of the trimeric HR assembly, a tilted homotrimer and a trimeric complex with bacterioruberin. A similar trimeric complex of archaerhodopsin-2 with bacterioruberin has been reported (16).

On the other hand, it has been recently reported that NpHR overexpressed in *Escherichia coli* cells, which has no bacterioruberin, has intermolecular interactions robust enough to retain its trimeric assembly upon the solubilization in a detergent DDM solution (8,9). Chloride binding and photocycle of NpHR expressed both in *E. coli* (17–23) and in *Natronomonas pharaonis* (24) cells are the same. However, the crystal structure of NpHR produced in *E. coli* has not been revealed. BR also forms a homotrimer in the membrane (2,6,7), however the trimeric structure dissociates into monomers when detergent has solubilized it (25–27).

According to these features, we supposed that the NpHR trimer in the absence of bacterioruberin is stabilized by the significant protein-protein interaction in the detergent solution; BR never has this interaction. However, the important factors for such a rigid trimeric formation of NpHR have not yet been determined. It is believed that the identification of the factors important for trimerization will allow us to discuss in detail the trimerization mechanisms and the regulation of the structural dynamics of NpHR in the presence and absence of bacterioruberin.

In this study, to elucidate the mechanism underlying the structural stabilization of the NpHR homotrimer in the detergent solution and the relationship between trimer formation and photoreactive function, we carried out some

spectroscopic and molecular size analyses. From comparison of the trimeric structures of HsHR and NpHR, we discovered that Phe^{150}, which is thought to be located at the central part of the NpHR trimer, has an important role in the stabilization of the assembly. The quantum-mechanical calculations also supported this finding, indicating that the dispersion energy contributes significantly to the equilateral triangular interactions of three Phe^{150} residues. We succeeded in preparing mono-, di-, and trimeric NpHR in detergent solution by a single mutation at the F-150th position to W, A, and Y, respectively, and the preparations enabled us to discuss the functional significance of trimerization. Flash photolysis spectroscopy on the trimer-dissociated mutants suggested that the trimeric assembly of NpHR was allowed to contribute to the regulation of functional dynamics during the photoreaction.

MATERIALS AND METHODS

Protein expression and purification

Wild-type (WT) NpHR and Y39A, W121A, F150A, F150W, F150Y, and W179A mutants were functionally expressed in *E. coli* BL21 (DE3) cells by reference to (1) and (17). The construction of the expression plasmid of WT NpHR with C-terminal 6 × His tag (pET21c(+)/NpHR-WT, Novagen, Madison, WI) was the same as reported previously (17). Sequences of primers for the mutants are summarized in Table S1 in the Supporting Material. The correctness of the mutated plasmids was confirmed by dideoxy sequencing (Applied Biosystems, Forster City, CA).

Measurement of the chloride-dependent shift in visible absorption spectra

Previously reported methods were used (18). Absorption spectra in the 250–750 nm regions were recorded at 25°C using UV-1800 UV spectrophotometer (Shimadzu, Kyoto, Japan). Samples were put into a 10 mm optical cuvette and scanned once. The baseline was collected with a buffer blank. Samples were dissolved in 10 mM MOPS buffer (pH 7, 0.1% DDM, Dojindo Lab, Kumamoto, Japan), and then NaCl was titrated up to 1 M.

CD spectroscopy

All the CD spectra in the 250–700 nm regions were recorded using a J-725 spectropolarimeter (Jasco, Tokyo, Japan). Two-time accumulation was carried out at a scanning speed of 200 nm/min and sensitivity of 20 mdeg at 25°C. The baseline was collected with a buffer blank. The path length of the optical cuvette was 10 mm. The absorption spectra of NpHRs, which were used for the calculation of K_d values in the ground state, were also obtained by converting a photomultiplier voltage signal of a CD apparatus into the optical density (log I_0/I) using a computer. Samples were dissolved in 10 mM MOPS buffer (pH 7, 0.1% DDM) containing 0.3 M Na_2SO_4, and then NaCl were titrated up to 1 M.

SEC and SDS-PAGE analysis of cross-linked NpHRs

SEC samples containing 20 μM NpHRs in 10 mM MOPS buffer (pH 7, 0.3 M NaCl, 0.1% DDM) were applied to a Superdex 200 10/300 GL size-exclusion column (GE Healthcare, UK, total bed volume; $V_t = 24$ (mL)) previously equilibrated with the same buffer. The Supporting Material section gives detailed descriptions.

Laser flash photolysis spectroscopy

A computer-controlled flash photolysis apparatus was constructed as described in previous studies (2,3). The transient absorption changes from 350 to 710 nm induced by a laser pulse were acquired at 0.5 ms between −44 and 220 ms. The data after 10 ms were fitted. The analyses of the photocycling data were performed as described previously (2–4). The Supporting Material section gives detailed descriptions.

Retinal composition analysis with normal-phase high-performance liquid chromatography (NP-HPLC)

The retinal compositions in the absence and presence of 0.5 M NaCl in light and dark states were analyzed by NP-HPLC, as described previously (5). The molar compositions of the retinal isomers were calculated from the areas of peaks in the HPLC patterns. Peaks were assigned by comparing the peaks with those in the HPLC pattern from retinal oximes extracted by the same method from BR kept in the dark.

Computational details

To estimate a homotrimeric NpHR structure in the absence of bacteriorubberin, the trimeric structure of HsHR, PDB code: 1E12 (3), was refined via an ab initio QM/MM geometry optimization (28,29) at the second-order Møller-Plesset perturbation (MP2)/Amber99 level of theory. The Supporting Material section gives detailed descriptions.

RESULTS

Identification of the important amino acids for homotrimer formation

Fig. 1, *A* and *B*, show the trimer models of HsHR and NpHR viewed from the cytoplasmic side. First, we predicted some amino acids, which were considered important for the homotrimer formation of NpHR in the absence of bacteriorubberin based on the contact surface area, and calculated as the difference in surface area between trimer and monomer. Fig. 1 *C* shows the contact surface of HsHR monomer, which shares high sequential homology with NpHR (whole structure; identity 55%, similarity 83%, and root mean-square deviation 0.69 Å, transmembrane domain; 65%, 92%, and 0.59 Å, respectively), suggesting that these HR monomers are expected to have similar surface structure especially in the transmembrane region that includes the contact surface. In the case of BR and visual rhodopsin, it was suggested that some aromatic residues contributed to the intermolecular interactions to retain their oligomeric assemblies (6,7,30). As we assume that NpHR obtained from *E. coli* membrane has a similar intermolecular interface to HsHR because of their homologies, we focused on three aromatic residues (Y39, F150, and W179) located on the interface as candidates for the key residue of NpHR trimerization. In addition, we focused on W121 of NpHR as

a candidate as well, which is not located at the contact region, because it was previously reported that W80 of BR corresponding to W121 played an important role in trimer formation (6,7). In the case of the HsHR trimer model (Fig. 1 *A*), the slightly tilted protomers form more compact assembly at the cytoplasmic interface. The aromatic side chain of each F150 residue face the central region of the trimer, and the distance from F150-Cδ in one monomer to F150-Cε in a neighboring monomer was estimated to be 4.59 Å, close for an equilateral triangular interaction of the aromatic rings within the trimeric interface of the protein. On the contrary, in the case of the trimeric NpHR-bacterioruberin complex model (Fig. 1 *B*), that was estimated to be 13.09 Å, which is too apart to contact with each aromatic rings. Sequence alignment in Fig. 1 *D* showed that F150 in NpHR is conserved in the HRs of various kinds of halophilic archaea and bacteria, and the rest of the four aromatic residues were also highly conserved. In this study, these aromatic residues were mutated to Ala.

In BR and HR, CD spectrum in the visible region has been used to help understand the property of retinal chromophore and, in turn, their trimeric assembly (8,9,17,31,32). Recent study has reported that the interaction between the chromophores in the assembly has an exciton coupling and significantly contributes to the CD shape (33). In the visible CD spectra in Fig. 2 *A*, NpHR-WT, Y39A, W121A, and W179A exhibited biphasic curves. In contrast, the biphasic curve was absent in the F150A mutant, which suggested that the NpHR trimer was dissociated (32). Therefore, we identified F150 as the key residue for the trimerization of NpHR.

Further structural analyses on F150 of NpHR

To elucidate the structural significance of F150, NpHR-F150W, and -F150Y mutants were additionally prepared. Fig. 2 *B* indicates that the biphasic visible CD spectra are observed in WT and F150Y, but not in F150A or F150W. These results suggest the dissociation of the trimer in not only F150A but also F150W. Interestingly, F150Y irreversibly lost the biphasic curve when it was treated with the buffer with low ionic strength. This finding may suggest that F150Y forms a trimer as well as WT, but the interaction to retain its trimeric assembly is weaker than that of WT. However, it is noted that the relationship between the biphasic CD spectrum and the oligomeric state of the archaeal rhodopsins is still controversial (34). Thus, the states of higher-order structure were investigated in detail using the following techniques.

The results of analytical SEC clearly assigned the states of the higher-order structures of WT and mutants: that is,

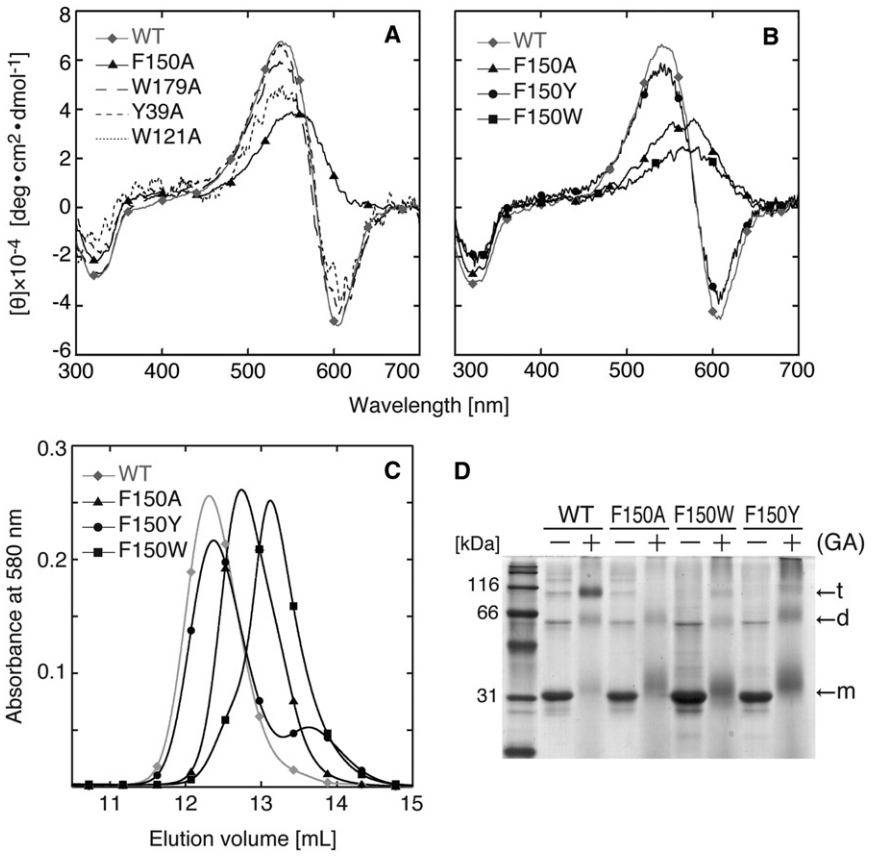

FIGURE 2 (*A* and *B*) Visible CD spectra of NpHR-WT and mutants. Proteins were solubilized in 10 mM MOPS buffer (pH 7, 0.3 M NaCl, 0.1% DDM) containing 0.3 M Na_2SO_4. Spectra were recorded at 25°C. (*A*) Representative amino acids correspond to those shown in Fig. 1. (*B*) Phenylalanine 150 of NpHR was additionally mutated into other aromatic residues, Tyr and Trp. (*C* and *D*) Molecular size analysis of NpHR-WT and F150 mutants. (*C*) Size-exclusion chromatograms of NpHRs. The samples containing 20 μM protein in 10 mM MOPS buffer (pH 7, 0.3 M NaCl, 0.1% DDM) were applied to the column. The program was run at a flow rate of 0.4 mL/min, and the eluting proteins were detected by the absorption at 580 nm. (*D*) SDS-PAGE analysis on cross-linked NpHRs. Cross-link was induced by the addition of 1% GA (9). Molecular mass of monomeric NpHR is ~32 kDa. Symbols − and + denote the absence and presence of GA; t, d, and m denote the trimer, dimer, and monomer, respectively.

WT as a trimer, F150A as a dimer, F150W as a monomer, and F150Y as a trimer including a small monomeric component, respectively (Fig. 2 *C*). For further analysis of the oligomeric state, SDS-PAGE was performed for each NpHR sample after cross-linking by GA (8). Fig. 2 *D* shows that WT is cross-linked and its main band emerges near the position of 116 kDa corresponding to the molecular mass of the trimer, indicating that WT forms a robust trimer in DDM. On the other hand, the series of F150 mutants was not all cross-linked and the main bands consequently emerged near the position of 31 kDa corresponding to the monomer.

All these results suggest that F150 is significant for retaining the robust trimeric assembly of NpHR in DDM solution. We succeeded in controlling the oligomeric state of NpHR by single mutation. It may be reasonable to suppose that the F150Y mutant contains a small monomeric component as an equilibrium state because the intermolecular interaction of this mutant is weak. The dimerization details of the F150A mutant are unexplained at present. Thus, further structural investigation focusing on the molecular orientation or the whole structure is needed.

Cl^--dependent absorption changes in the ground state

To elucidate the relationship between trimer formation and photoreaction of NpHR, several spectroscopic and chromatographic analyses were performed. Here, we focused on the functional features of NpHR in the ground state. The wavelength of maximum absorption (λ_{max}) is summarized in Table 1. It is known that the λ_{max} of WT is 578 nm in the presence of Cl^- and 600 nm in the absence of Cl^-. In this study, the λ_{max} values of all F150 mutants were also 578 nm in the presence of Cl^- but 573 nm in the absence of Cl^-, suggesting that a subtle structural change in the retinal environment may be induced by the dissociation of the trimers in the absence of Cl^-. Note that the F150Y trimer is dissociated as indicated by the visible CD spectra in Fig. S1 because the sample has been desalted before the absorption measurements. The extinction coefficient of F150 mutants increased by Cl^- binding to the vicinity of the retinal Schiff base as well as WT (36). Moreover, the absorption bands of F150 mutants with λ_{max} of 573 nm in the absence of Cl^- were red-shifted to 591 nm in F150A and F150W, and to 598 nm in F150Y, by the addition of 0.3 M SO_4^{2-} although λ_{max} of WT was not changed (data not shown). These results may suggest that binding of SO_4^{2-} to some specific site leads to change of the retinal environment.

In previous studies, the affinity of NpHR to Cl^- was examined by the absorption change resulting from the Cl^- titration experiment (17). We plotted the absorption changes at 633 nm, at which the change in difference spectra is the greatest, as a function of the Cl^- concentration, and then applied the data to Eq. S1. The resultant $K_{d(Cl^- \text{ bind})}$ values and Hill coefficients are summarized in Table 1. Because the values ranged in the same order, we concluded that F150 mutants had the same affinity for Cl^- as WT in the ground state.

Transient absorption change analysis with laser flash photolysis spectroscopy

Photocycle overview

The photocycle and related kinetic parameters of NpHR-WT and F150 mutants were investigated using flash photolysis spectroscopy. Fig. 3, *A–D*, show the flash-induced transient absorption changes in NpHRs under the 1 M Cl^- condition. The data were exponentially fitted by four photochemically defined states, such as P1 (L1), P2 (L2), P3 (equilibrium between N and O), and P4 (NpHR′). In all of the samples, despite the oligomeric states, the absorption changes were restored to zero at tens of milliseconds. However, several differences were observed in the photoreaction property between the trimeric NpHRs (WT and F150Y) and the trimer-dissociated ones (F150A and F150W).

In the changes at 650 nm, which describes the genesis and the decay of O, the relative peak intensity decreased in the trimer-dissociated mutants at higher Cl^- concentrations. The time constants τ_1–τ_4 at 1 M NaCl is shown in Fig. 3 *E*. No drastic changes of each time constant by the mutation were analyzed although a slight increasing of the decay speed of the early intermediate L1, L2 (τ_1, τ_2) of F150A was observed. It has been reported that the L1 to L2 or L2 to N transition of NpHR indicates an accessibility change of the anion from the extracellular to the cytoplasmic side, suggesting that Cl^- movement inside the molecule occurs at the early stage of the photocycle (19,35). These facts may be related to the trimer dissociation.

TABLE 1 Summary of λ_{max} in the absence and presence of 1 M NaCl, and K_d values in the ground and photoexcited states

	λ_{max} (nm)		Ground state (Cl^- bind)		Photoexcited state (Cl^- release)	
Proteins	0 M NaCl	1 M NaCl	K_d (mM) (SE)	Hill coef. (SE)	K_d (mM) (SE)	Hill coef. (SE)
WT	600	578	1.70 (0.093)	0.90 (0.040)	1200*	–
F150A	573	578	2.62 (0.15)	1.0 (0.058)	64.2 (1.08)	0.95 (0.017)
F150W	573	578	4.06 (0.12)	0.93 (0.022)	200 (0.029)	0.70 (0.089)
F150Y	573	578	1.37 (0.036)	0.82 (0.017)	922 (0.103)	0.97 (0.10)

SE, standard error.

*(19) Hasegawa et al.; (39) Chizhov et al.

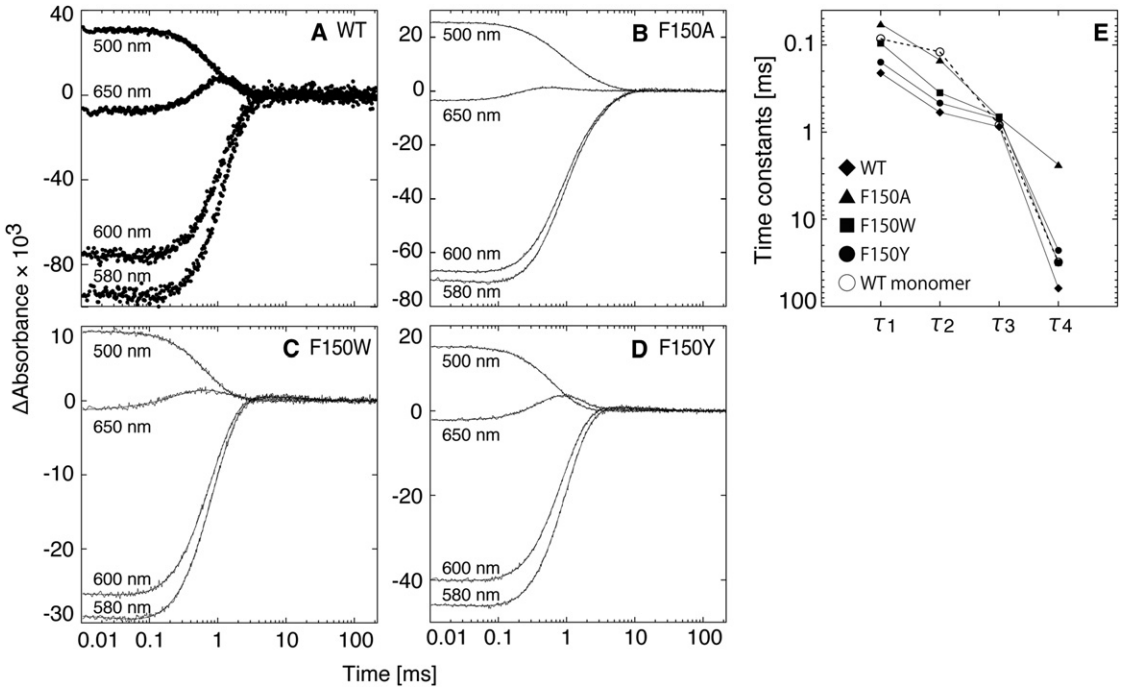

FIGURE 3 Flash-induced transient absorption changes of NpHR-WT and F150 mutants at typical wavelengths. (*A–D*) The absorption changes in the presence of 1 M NaCl. Proteins were solubilized in 10 mM MOPS buffer (pH 7, 1 M NaCl, 0.1% DDM). All measurements were performed at 20°C. (*E*) Time constants in the photocycle in the presence of 1 M NaCl. The values were obtained from the global fitting analysis on the data shown in the spectra *A–D*.

Cl^--dependent absorption changes in the photoexcited intermediates

The data from flash photolysis spectroscopy were fitted with the conventional four components. It is known that the Cl^--dependent absorption changes are observed in the P3 state, which corresponds to the equilibrium of N (520 nm) and O (650 nm), and is important for Cl^- release from the molecule. The absorption changes of F150 mutants are shown in Fig. 4, *A–C*. As in past studies, the equilibrium state was shifted from O to N when the Cl^- concentration was increased. However, the magnitude of the change varied from mutant to mutant. Fig. 4 *D* shows the fraction of N against the Cl^- concentration. The fraction followed sigmoidal curves, and the curves were fitted with Eq. S4. The resultant $K_{d(Cl^-\ release)}$ values and Hill coefficients are summarized in Table 1. In the case of WT, the K_d value is known to rise from the order of millimolar to that of molar when the Cl^- binding to the protein in the ground state is released in the photoexcited state. However, in the trimer-dissociated mutants, $K_{d(Cl^-\ release)}$ values became much smaller, which ranged from tens of millimolars to a few hundreds of them, and than the trimers, indicating the strong affinity to Cl^- in the photoexcited state.

Interestingly, the Cl^--dependent spectral changes were also observed in the P4 state, which corresponds to NpHR′ exhibiting λ_{max} of 578 nm, the same as the ground state of the trimer-dissociated mutants (Fig. 4, *E* and *F*). In these mutants at lower Cl^- concentrations, the contribution of the component at longer wavelength seemed to remain. This component is thought to be O. Therefore, the result suggested that the equilibrium state between O and NpHR′ was newly appeared in the mutants. With the increase in Cl^- concentration, the equilibrium shifted to NpHR′. Especially in the case of F150A, the contribution of the component at shorter wavelengths emerged at higher Cl^- concentrations. Because this component is thought to be N, the P4 spectra of the trimer-dissociated mutants include the previous, which is in the case of F150A, and the following intermediates in the photocycle and show the equilibrium among two or three components, which WT has never shown. In these respects, it is suggested that the native-trimeric assembly contributes to the efficient generation of photointermediate structures that act as a Cl^- pump during the photocycle. The question is whether some of the phenotypes reported in this study are caused directly by the mutation or by change of the protein-protein interaction. Further investigation may be needed to obtain quantitative differences between trimer and monomer.

DISCUSSION

Structural importance of F150 for homotrimer formation of NpHR

BR, which is a proton pump that forms a trimeric assembly on the native purple membrane, has been known to be dissociated into a monomer by detergents such as Triton

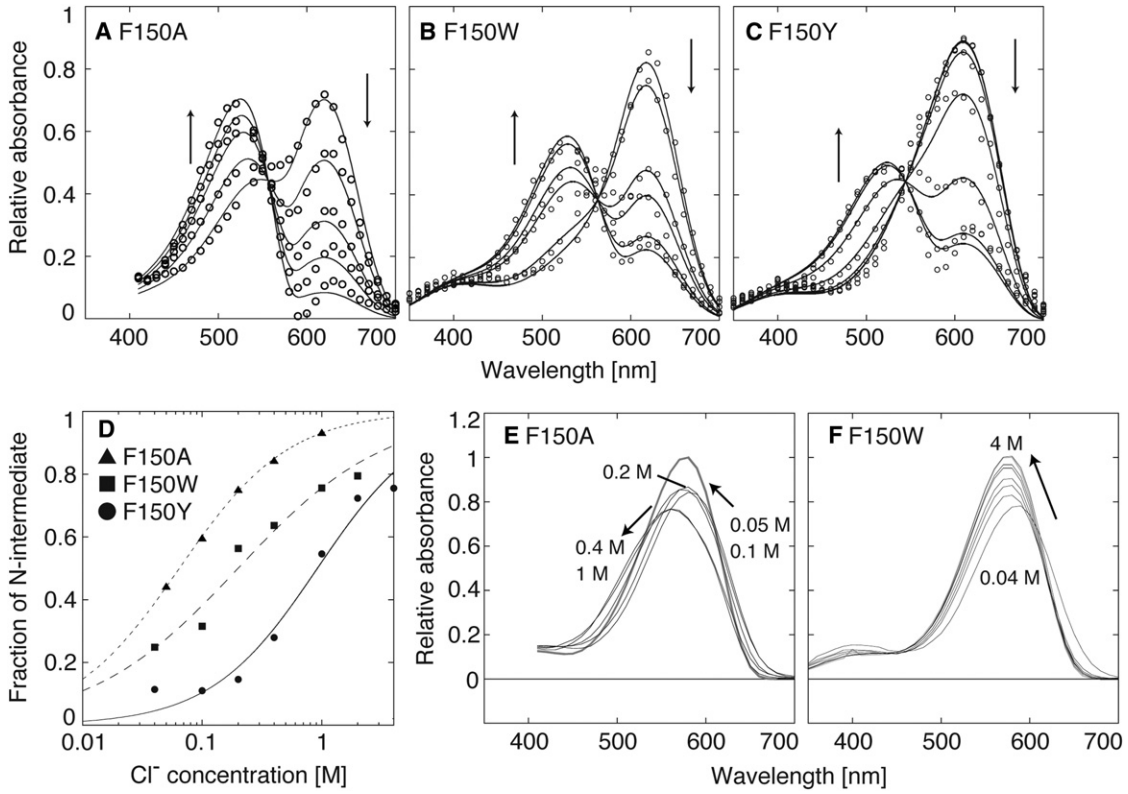

FIGURE 4 (*A–C*) Multi-Gaussian fit of the P3 state of NpHR mutants. The absolute spectra of this state at various Cl^- concentrations (*open circles*) were fitted in the same way as previously reported (19). Chloride-dependent absorption changes in the photo-excited N and O observed in the P3 spectra of F150 mutants. The samples were titrated with NaCl from 0.04 to 4 M. The arrows indicated the changes in the accumulation of N (520 nm) and of O (600 nm). (*D*) Chloride-dependent changes in the absorbance at 520 nm, which represents the fraction of N, of F150 mutants shown in spectra *A–C*. (*E* and *F*) Chloride-dependent absorption changes in the photoexcited NpHR′ observed in P4 spectra of (*E*) NpHR-F150A and (*F*) F150W. The arrows indicate the spectral shift resulting from the addition of Cl^-.

X-100 and octyl-β-D-glucoside (25,26). Similarly, visual rhodopsin is also dissociated when the protein is solubilized from the rod cell membrane by DDM (36). On the other hand, NpHR trimer functionally expressed on the *E. coli* membrane is able to retain its trimeric structure even after solubilization by a high concentration of the detergents in the presence of NaCl (8,9,37).

In this mutation work, we determined that Phe^{150} of NpHR is a structurally important residue for homotrimer formation. It is perfectly conserved among HR molecules of any species. On the other hand, it is not conserved in BR, which has L109 instead of F150. From the structural model of HsHR homotrimer (the distance from F150-Cδ in one monomer to F150-Cε in a neighboring monomer was estimated to be 4.59 Å), it has been speculated that F150 residues of three NpHR protomers are close enough to interact with each other in the trimer (Fig. 1 *A*). It has been reported that visual rhodopsin shows the same tendency as NpHR on the specific interaction between aromatic residues or between aromatic and polar residues at the protein interface (30). Furthermore, it has been reported that W80 of BR interacts with a specific archaeal glycolipid located in the center of the BR trimer, and this interaction helps to retain the trimeric formation (6,7). In this study, however, the mutation of W121 of NpHR corresponding to W80 of BR into A did not influence the trimeric formation (Fig. 2 *A*). It is plausible that there is no interaction between lipids and aromatic residues in NpHR, unlike BR. Two other mutants, Y39A and W179A, also retained the trimeric structure, although these are located at the molecular interface (Fig. 1 *C*), suggesting that these residues are not important for trimer formation and preservation.

The single mutation into F150 resulted in three different oligomeric assemblies: F150W as a monomer, F150A as a dimer, and F150Y as a weak trimer (Fig. 2, *B* and *C*). It was previously reported that monomeric WT reassembles into a trimer under the conditions of high ionic strength and low DDM concentration (<0.1%) (9). In the case of the F150W mutant, the biphasic CD spectrum was not observed in both the presence and absence of NaCl (Fig. 2 *B*), suggesting that the monomeric F150W never reassembled into a trimer.

Fig. 5 shows the electrostatic potential maps of QM/MM optimized structures of trimeric interaction between the F150 side chains in WT, F150A, F150W, and F150Y, which were calculated based on the compact HR homotrimer

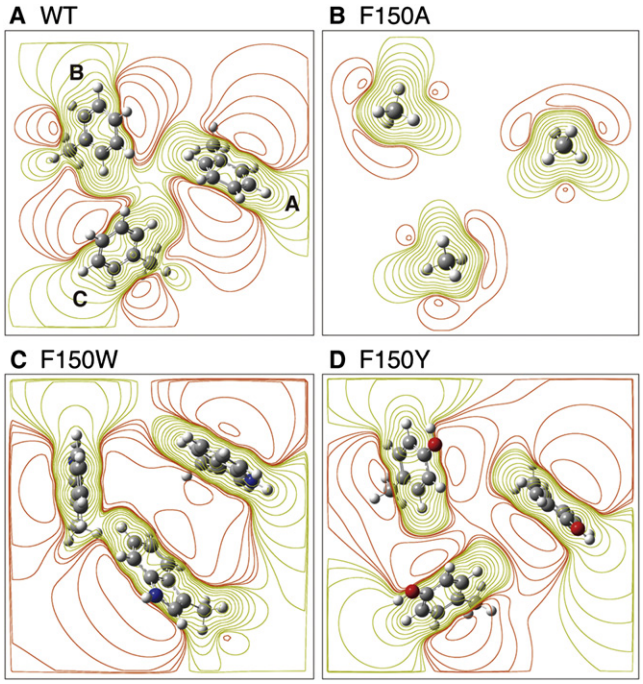

FIGURE 5 Electrostatic potential maps of QM/MM optimized NpHR model structures of (*A*) phenylalanines in WT, (*B*) alanines in F150A, (*C*) tryptophans in F150W, and (*D*) tyrosines in F150Y. The green and red areas represent positively and negatively charged potential energy, respectively. Computational details are described in the Supporting Material.

model. (see the Supporting Material section for detailed descriptions). As shown in Fig. 5, the distribution of electrostatic potential in F150Y is similar to that in WT, which also suggests that F150Y has the same kinds of interactions as WT. The electrostatic potential in F150A has a small distribution compared with the other proteins, which is attributed to the small side chain of alanine. The steric hindrance of a larger tryptophan and the repulsive interaction indicated by the QM calculation may contribute to the dissociation in F150W. On the other hand, ionic strength strongly affected the oligomeric state of F150Y mutants (Fig. S1). In this case, the biphasic CD was lost under the low ionic strength condition and its trimeric assembly was never restored even after the addition of 0.3 M NaCl. These results lead to the possibility that the strong packing interaction among NpHR molecules is caused by the equilateral triangular interactions of three Phe^{150} side chains. The theoretical investigation in this study suggested that the structural symmetry and the interaction originating from the dispersion energy, which was calculated quantum mechanically, contribute to the trimer stabilization (Tables 2 and Table S2).

The substitution of F150 with smaller amino acids also induced the trimer dissociation. A size-exclusion chromatogram showed the F150A mutant dissociates a trimer into a dimer (Fig. 2 *C*). A visible CD experiment also supported the dissociation of the trimers (Fig. 2 *B*). However, the

TABLE 2 Summary of the trimeric interaction energies calculated with QM

		E_{int} (kcal/mol)		Decomposition (kcal/mol)	
Proteins	QM site	CCSD	HF	Disp.	Others
WT	A-B-C	−1.29	−0.56	−0.73	−0.57
F150A		−0.01	0.00	−0.01	−0.01
F150W		−1.86	1.35	−3.21	1.36
F150Y		−0.50	−0.24	−0.26	−0.24

A-B-C, trimer interaction; CCSD, CCSD/6-31g(d) interaction energy; HF, Hartree-Fock/6-31g(d) interaction energy; Disp., dispersion energy. Detailed information is listed in Table S2.

assembling structure such as molecular orientation in the dimer is unknown. We should note that the intermolecular interaction occurs not only at the 150th position but also at another extensive contact surface area. We concluded that the preservation of the homotrimeric assembly requires the intermolecular interaction in which some amino acids on the molecular surface engage, and that F150 makes the largest contribution to the interaction among these amino acids.

Trimer formation leads to significant changes in photoreaction

In the ground state, the characteristics of NpHR-WT and F150 mutants in the presence of Cl^- were almost the same in terms of λ_{max}, $K_{d\ (Cl^-\ bind)}$ values and retinal isomer composition (Table 1 and Fig. S4). These results suggest that the effect of the mutation is minor to the retinal environment in the ground state of Cl^--bound NpHR, although only the local intermolecular interaction between NpHR molecules has been destroyed.

On the other hand, λ_{max} of all three F150 mutants was 574 nm in the absence of Cl^- and red-shifted to 578 nm in the presence of Cl^-. This behavior was opposite that of trimeric WT (Table 1). These results suggest that the influence of the lack of intermolecular interaction among NpHR monomers appears in the Cl^--free condition with the change in the retinal environment. It has been reported that the spectral blue shift of BR by dissociation into monomers has been caused by environmental changes, such as a change in the charge state in Asp^{85}, the counterion of the protonated Schiff base (38). A similar phenomenon may have happened in the retinal environment of monomerized NpHR without Cl^-.

The trimer-dissociated F150A and F150W mutants exhibited some changes in their photocycles, which were closely connected to the Cl^--pumping activity. The main characteristics are i), the decrease in the accumulation of O (Fig. 3), ii), the decrease in the $K_{d\ (Cl^-\ release)}$ values (Fig. 4 *D*), and iii), inefficient recovery to the ground state from NpHR′ (Fig. 4, *E* and *F*). The facts i) and ii) mean that the accumulation of O is suppressed because

the transition from N to O is suppressed by the strong affinity to Cl^- at this transient stage. Based on the results of flash photolysis spectroscopy, we propose two possible photoreaction schemes of the trimer-dissociated NpHRs (Fig. 6). As mentioned previously, it is plausible that the P4 spectra representing NpHR′ additionally contained contributions from previous components O and N, and showed the equilibrium among these components (I). Fig. 6 summarizes the scheme in which the contribution of the transition from O to N of these mutants becomes larger than that of the WT protein and that from NpHR′ to O begins to emerge. Especially in the case of the F150A mutant (Fig. 4 *A*), the contribution of N becomes stronger at high concentrations of Cl^-. This fact may suggest that the NpHR-F150A shows the photocycle with the branched pathway (II). At high Cl^- concentration, it was revealed from P3 and P4 spectra (Fig. 4, *A* and *E*), that the equilibrium was shifted largely to N. In this case, N and NpHR′ can be considered to be in equilibrium, judging from P4 spectra in Fig. 4 *E*.

Considering that O and N are also in equilibrium, NpHR′, which is in equilibrium with N, can be renamed as NpHR,″ which has the same λ_{max} as NpHR′ and is branched from the normal photoreaction scheme that trimeric NpHR shows. N and NpHR″ retain Cl^- inside the molecule; therefore, trimer-dissociated NpHR does not transport Cl^- in this pathway. Hackmann and co-workers (35) reported that the photocycle of NpHR at high Cl^- concentration branches off into two reaction pathways: one is normal and the other inhibits Cl^- transport. In our model, we defined N, which comes up after L2 and is in equilibrium with the next O, and proposed that the new NpHR″ branched off from the former N. We understand that the branching L2′-intermediate, which those authors proposed, corresponded to NpHR″ in our model.

The differences in photochemical properties of the two trimer-dissociated mutants were observed as mentioned previously. However, it is difficult to currently clear these differences. It may be supposed that the characteristic of F150A mutant results from the change in the local structural flexibility (space) by the mutation into alanine with a small side chain, and its dimeric assembly that is retained by a nonspecific intermolecular interaction. Further study should be carried out taking into account the effect of the mutation and the dimeric state of F150A mutant.

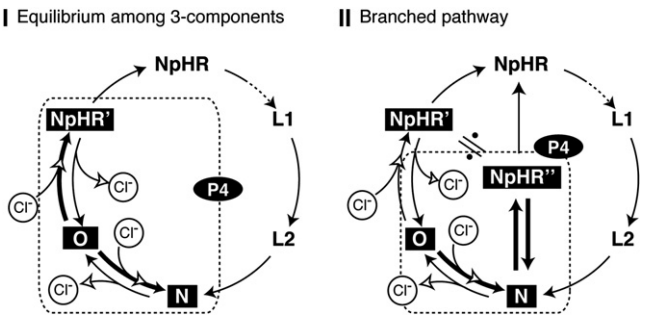

FIGURE 6 Possible schemes of the photocycle estimated from the data on NpHR-F150A and F150W. (I) Equilibrium among three components, (II) Branched pathway.

CONCLUSION

We conclude that Phe^{150}, which is located at the interface of NpHR monomers expressed in *E. coli* cells, is a significant contributor to self-assembling of the homotrimer. Moreover, the trimeric structure of NpHR is significant for its photoreaction dynamics, which produce the transient structure as appropriate photointermediates. We can speculate that bacterioruberin is also effective for modulation of the NpHR trimer assembly.

SUPPORTING MATERIAL

Detailed descriptions, four figures, two tables, and references are available at http://www.biophysj.org/biophysj/supplemental/S0006-3495(12)00561-9.

This study was partially supported by Grants-in-Aid for Scientific Research in Priority Areas and the National Project on Targeted Protein Research Program from the Ministry of Education, Culture, Sports, Science, and Technology of Japan. One of the authors (K.F.) gratefully acknowledges a Grant-in-Aid for Young Scientists (B) from the Japan Society for the Promotion of Science.

REFERENCES

1. Spudich, J. L., C. S. Yang, …, E. N. Spudich. 2000. Retinylidene proteins: structures and functions from archaea to humans. *Annu. Rev. Cell Dev. Biol.* 16:365–392.
2. Essen, L. O., R. Siegert, …, D. Oesterhelt. 1998. Lipid patches in membrane protein oligomers: crystal structure of the bacteriorhodopsin-lipid complex. *Proc. Natl. Acad. Sci. USA.* 95:11673–11678.
3. Kolbe, M., H. Besir, …, D. Oesterhelt. 2000. Structure of the light-driven chloride pump halorhodopsin at 1.8 A resolution. *Science.* 288:1390–1396.
4. Kouyama, T., S. Kanada, …, K. Ihara. 2010. Crystal structure of the light-driven chloride pump halorhodopsin from *Natronomonas pharaonis*. *J. Mol. Biol.* 396:564–579.
5. Gordeliy, V. I., J. Labahn, …, M. Engelhard. 2002. Molecular basis of transmembrane signalling by sensory rhodopsin II-transducer complex. *Nature.* 419:484–487.
6. Sapra, K. T., H. Besir, …, D. J. Muller. 2006. Characterizing molecular interactions in different bacteriorhodopsin assemblies by single-molecule force spectroscopy. *J. Mol. Biol.* 355:640–650.
7. Weik, M., H. Patzelt, …, D. Oesterhelt. 1998. Localization of glycolipids in membranes by in vivo labeling and neutron diffraction. *Mol. Cell.* 1:411–419.
8. Sasaki, T., M. Kubo, …, M. Demura. 2009. Halorhodopsin from *Natronomonas pharaonis* forms a trimer even in the presence of a detergent, dodecyl-β-D-maltoside. *Photochem. Photobiol.* 85:130–136.
9. Sasaki, T., T. Aizawa, …, M. Demura. 2009. Effect of chloride binding on the thermal trimer-monomer conversion of halorhodopsin in the solubilized system. *Biochemistry.* 48:12089–12095.
10. Schobert, B., and J. K. Lanyi. 1982. Halorhodopsin is a light-driven chloride pump. *J. Biol. Chem.* 257:10306–10313.
11. Váró, G. 2000. Analogies between halorhodopsin and bacteriorhodopsin. *Biochim. Biophys. Acta.* 1460:220–229.

12. Gradinaru, V., K. R. Thompson, and K. Deisseroth. 2008. eNpHR: a *Natronomonas* halorhodopsin enhanced for optogenetic applications. *Brain Cell Biol.* 36:129–139.

13. Diester, I., M. T. Kaufman, …, K. V. Shenoy. 2011. An optogenetic toolbox designed for primates. *Nat. Neurosci.* 14:387–397.

14. Kunji, E. R. S., S. von Gronau, …, R. Henderson. 2000. The three-dimensional structure of halorhodopsin to 5 A by electron crystallography: a new unbending procedure for two-dimensional crystals by using a global reference structure. *Proc. Natl. Acad. Sci. USA.* 97:4637–4642.

15. Ihara, K., A. Narusawa, …, T. Kouyama. 2008. A halorhodopsin-overproducing mutant isolated from an extremely haloalkaliphilic archaeon *Natronomonas pharaonis*. *FEBS Lett.* 582:2931–2936.

16. Yoshimura, K., and T. Kouyama. 2008. Structural role of bacterioruberin in the trimeric structure of archaerhodopsin-2. *J. Mol. Biol.* 375:1267–1281.

17. Sato, M., T. Kanamori, …, K. Nitta. 2002. Stopped-flow analysis on anion binding to blue-form halorhodopsin from *Natronobacterium pharaonis:* comparison with the anion-uptake process during the photocycle. *Biochemistry.* 41:2452–2458.

18. Sato, M., M. Kubo, …, M. Demura. 2005. Role of putative anion-binding sites in cytoplasmic and extracellular channels of *Natronomonas pharaonis* halorhodopsin. *Biochemistry.* 44:4775–4784.

19. Hasegawa, C., T. Kikukawa, …, N. Kamo. 2007. Interaction of the halobacterial transducer to a halorhodopsin mutant engineered so as to bind the transducer: Cl^- circulation within the extracellular channel. *Photochem. Photobiol.* 83:293–302.

20. Inoue, K., M. Kubo, …, M. Terazima. 2009. Reaction dynamics of halorhodopsin studied by time-resolved diffusion. *Biophys. J.* 96:3724–3734.

21. Seki, A., S. Miyauchi, …, N. Kamo. 2007. Heterologous expression of *Pharaonis* halorhodopsin in *Xenopus laevis* oocytes and electrophysiological characterization of its light-driven Cl- pump activity. *Biophys. J.* 92:2559–2569.

22. Nakashima, K., T. Nakamura, …, H. Kandori. 2009. Property of anion binding site of *pharaonis* halorhodopsin studied by ultrafast pump-probe spectroscopy and low-temperature FTIR spectroscopy. *J. Phys. Chem.* 113:8429–8434.

23. Nakamura, T., S. Takeuchi, …, T. Tahara. 2008. Ultrafast pump-probe study of the primary photoreaction process in *pharaonis* halorhodopsin: halide ion dependence and isomerization dynamics. *J. Phys. Chem. B.* 112:12795–12800.

24. Scharf, B., and M. Engelhard. 1994. Blue halorhodopsin from *Natronobacterium pharaonis:* wavelength regulation by anions. *Biochemistry.* 33:6387–6393.

25. Dencher, N. A., and M. P. Heyn. 1978. Formation and properties of bacteriorhodopsin monomers in the non-ionic detergents octyl-β-D-glucoside and Triton X-100. *FEBS Lett.* 96:322–326.

26. Sasaki, T., M. Sonoyama, …, S. Mitaku. 2005. Photobleaching of bacteriorhodopsin solubilized with triton X-100. *Photochem. Photobiol.* 81:1131–1137.

27. Sasaki, T., M. Demura, …, Y. Mukai. 2011. Sensitive detection of protein-lipid interaction change on bacteriorhodopsin using dodecyl β-D-maltoside. *Biochemistry.* 50:2283–2290.

28. Warshel, A., and M. Levitt. 1976. Theoretical studies of enzymic reactions: dielectric, electrostatic and steric stabilization of the carbonium ion in the reaction of lysozyme. *J. Mol. Biol.* 103:227–249.

29. Fujimoto, K., and W.-T. Yang. 2008. Density-fragment interaction approach for quantum-mechanical/molecular-mechanical calculations with application to the excited states of a $Mg(^{2+})$-sensitive dye. *J. Chem. Phys.* 129:054102.

30. Salom, D., D. T. Lodowski, …, K. Palczewski. 2006. Crystal structure of a photoactivated deprotonated intermediate of rhodopsin. *Proc. Natl. Acad. Sci. USA.* 103:16123–16128.

31. Heyn, M. P., P.-J. Bauer, and N. A. Dencher. 1975. A natural CD label to probe the structure of the purple membrane from *Halobacterium halobium* by means of exciton coupling effects. *Biochem. Biophys. Res. Commun.* 67:897–903.

32. Yamashita, Y., T. Kikukawa, …, M. Demura. 2011. Expression of *salinarum* halorhodopsin in *Escherichia coli* cells: solubilization in the presence of retinal yields the natural state. *Biochim. Biophys. Acta.* 1808:2905–2912.

33. Pescitelli, G., and R. W. Woody. 2012. The exciton origin of the visible circular dichroism spectrum of bacteriorhodopsin. *J. Phys. Chem. B.* In press.

34. Karnaukhova, E., C. Vasileiou, …, B. Borhan. 2006. Circular dichroism of heterochromophoric and partially regenerated purple membrane: search for exciton coupling. *Chirality.* 18:72–83.

35. Hackmann, C., J. Guijarro, …, F. Siebert. 2001. Static and time-resolved step-scan Fourier transform infrared investigations of the photoreaction of halorhodopsin from *Natronobacterium pharaonis*: consequences for models of the anion translocation mechanism. *Biophys. J.* 81:394–406.

36. Jastrzebska, B., T. Maeda, …, K. Palczewski. 2004. Functional characterization of rhodopsin monomers and dimers in detergents. *J. Biol. Chem.* 279:54663–54675.

37. Kubo, M., M. Sato, …, M. Demura. 2005. Disassembling and bleaching of chloride-free *pharaonis* halorhodopsin by octyl-β-glucoside. *Biochemistry.* 44:12923–12931.

38. Wang, J., S. Link, …, M. A. El-Sayed. 2002. Comparison of the dynamics of the primary events of bacteriorhodopsin in its trimeric and monomeric states. *Biophys. J.* 83:1557–1566.

39. Chizhov, I., and M. Engelhard. 2001. Temperature and halide dependence of the photocycle of halorhodopsin from *Natronobacterium pharaonis*. *Biophys. J.* 81:1600–1612.